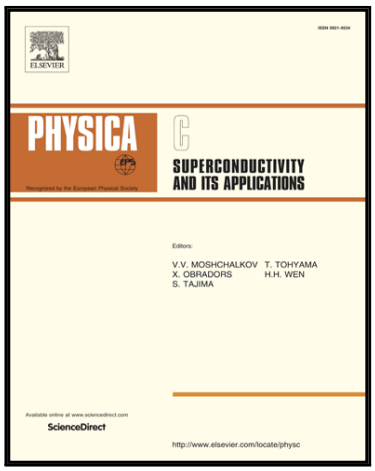

Guided vortex motion in dilute strong pinning environment: models and experiment

V.V. Guryev , S.V. Shavkin , V.S. Kruglov

PII: S0921-4534(22)00068-5
DOI: https://doi.org/10.1016/j.physc.2022.1354080
Reference: PHYSC 1354080

To appear in: *Physica C: Superconductivity and its applications*

Received date: 21 March 2022
Revised date: 16 May 2022
Accepted date: 31 May 2022

Please cite this article as: V.V. Guryev , S.V. Shavkin , V.S. Kruglov , Guided vortex motion in dilute strong pinning environment: models and experiment, *Physica C: Superconductivity and its applications* (2022), doi: https://doi.org/10.1016/j.physc.2022.1354080

Guided vortex motion in dilute strong pinning environment: models and experiment

V.V. Guryev, S.V. Shavkin, V.S. Kruglov
NRC Kurchatov institute, Kurchatov sq.1, 123182 Moscow, Russia

Highlights

- A brief overview of models predicting guiding angles is given.
- The guiding effect has been experimentally studied depending on the magnetic field magnitude and the excitation current on the Nb-Ti tape with rarefied α-Ti particles – strong pinning centers.
- The experimental data and models are compared. The model that describes the experiment most accurately is chosen.
- It is shown that the guiding experiments can serve as a tool to distinguish between plastic and elastic flux flow modes.

This article provides a brief overview of existing models that describe the guided flux motion phenomenon. The first model was proposed by Niessen et al. This original model utilizes the single-vortex approximation and provides a qualitative explanation of the effect; however, in most cases it provides an overestimated guiding angle. A second stochastic model explains the experimentally observed guiding angle decreasing (so-called "slipping effect") by the influence of thermal fluctuations. However, the performed estimations show that thermal fluctuations should not be significant. Another model for predicting the guiding angle is the anisotropic pinning model. This model operates in the critical state approximation, and the slipping effect is the combined action of anisotropic pinning and vortex interaction. The predictions of all three models were experimentally tested on a wide superconducting Nb-Ti tape containing 6% by volume ratio of α-Ti particles that act as strong pinning centers. The number of samples was sliced at different angles to the rolling direction to control the driving force direction with respect to the principal material directions. The transverse and longitudinal components of the electrical field were measured simultaneously in a perpendicular magnetic field with increasing transport current. It was found that when the generated electric field was sufficiently small, the guiding angle varied significantly at different locations along the sample. In this case, the anisotropic pinning model predicted the guiding angle averaged over the sample length. With a further increase in the transport current (and driving force), the guiding angle became uniform along the sample.

I. INTRODUCTION

In light of recent progress in quantum technology [1, 2] a field of science, which is often called "fluxonics" [3, 4] acquires particular relevance [5, 6, 7, 8, 9]. This name was given by analogy with electronics, since its basic element is the magnetic flux quantum - fluxon. One of the key tools of fluxonics is the guided flux motion (guiding) effect [4] a detailed description of which is given below. Generally speaking, the guiding effect is an essential attribute for any type II superconductors with anisotropic pinning, including practical superconductors for high current applications. The guiding effect is determined by the quantum nature of superconductivity. This effect manifests itself as a non-coincidence of the electric field and current density directions and, so, contributes to the tensor character

of the superconductor material equation [10], and consequently it should be taken into account in superconducting device design.

Let us consider the case of a superconducting platelet with a transport current density $\vec{j}$ in the external perpendicular magnetic field $\vec{H}$. The magnetic field is assumed to be strong enough to satisfy the condition for the magnetic induction $\vec{B} \approx \mu_0 \vec{H}$. The current acts on the vortex matter with the driving force (Fig. 1):

$$\vec{F} = [\vec{j} \times \vec{B}] \tag{1}$$

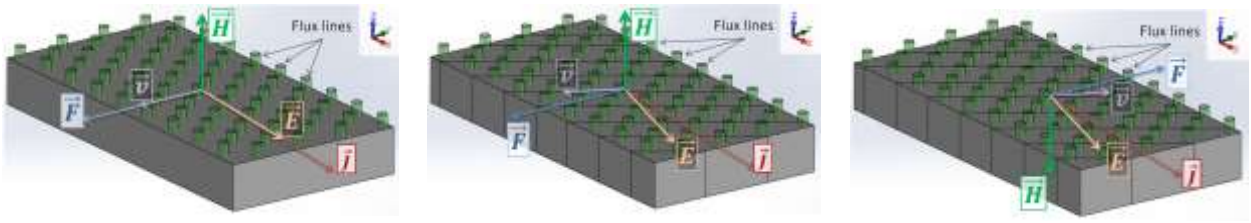

a b c

Fig. 1. Schematic representation of the vortices motion under the action of force $\vec{F}$ (1) (the magnetic field $\vec{H}$ is applied normal to the tape). For contrast, the vortices are depicted in green. a) The simple case when $\vec{F} \| \vec{v}$ ($\vec{j} \| \vec{E}$); b) the case when $\vec{F} \nparallel \vec{v}$; c) The case is similar to *b*, but with the inverted direction of the magnetic field $\vec{H}$.

This force leads to the vortices movement with an average velocity $\vec{v}$, which generates electrical voltage $\vec{E}$ (Fig. 1a):

$$\vec{E} = [\vec{B} \times \vec{v}] \tag{2}$$

Structural inhomogeneities (defects) in material impede the vortices motion. This is described by a pinning force opposite to the force (1). In the general case, if the defect shape is not globular and the distribution is not uniform, the pinning is anisotropic. Moreover, the anisotropy reveals itself not only in relation to magnetic field $\vec{B}$ direction but also in relation to the driving force (1) direction (which depends both on magnetic field $\vec{B}$ and the current $\vec{j}$). For example, pinning in the system of correlated parallel planar grain boundaries, such as in cold-rolled tapes, is anisotropic (in both the abovementioned senses). Anisotropy with respect to force (1) is due to the fact that the pinning force is smaller when flux moves along grain boundaries than when flux moves across these boundaries [11]. As a result, if the direction $\vec{F}$ is intermediate between two extreme cases (not along grain boundaries, nor across them), then the average velocity of vortices $\vec{v}$ will not be co-directed with the driving force (1): $\vec{v} \nparallel \vec{F}$. This situation is illustrated in Figure 1b. The electric field is still determined by (2), which leads to corresponding declination of the electric field against current density vector $\vec{E} \nparallel \vec{j}$. This forms a component of the electric field $E_\perp$ transverse to the transport current. We define the guiding angle as:

$$\beta = \operatorname{atan} \frac{E_\perp}{E_\parallel} \tag{3}$$

where $E_\perp$ and $E_\parallel$ are transverse and longitudinal components of the electric field to the transport current.

When the magnetic field direction is reversed the electric field does not change sign (see Fig. 1c). Thus, the transverse component of the electric field $E_\perp$, caused by the guiding effect is even with respect to the magnetic field inversion. This is an important distinction from the Hall effect (which is odd with respect to the magnetic field inversion) that allowed Nissen et al. to detect experimentally this effect on rolled Nb sheets, cold-rolled Pb–In alloys [12] and Nb–Ta alloys [13] in the 60s. In [13], a model was proposed that qualitatively explains the observed features, which is hereinafter referred to as a «primal model» (PM). Starting from these first experiments, it was clear that the pinning anisotropy is the origin of the guiding, but in most cases the direction of the vortex matter motion differs significantly from the «easiest motion» direction (e.g. along the grain boundaries) caused by the finite probability for the vortex moves across the grain boundaries (the so-called slipping effect). After Nissen's pioneering work, the

effect of guided flux motion has been repeatedly observed both in conventional superconductors with weak pinning [14, 15] and in HTS materials [16, 17, 18, 19]. However, the case of strong pinning, which is most interesting from a practical point of view, is poorly presented in the literature.

Hereafter we overview existing models explaining the features of the guided vortices motion (Section II), present the experimental results of the guiding-effect study in case of Nb-Ti tape containing up to 6 vol. % of α-Ti particles, which act as strong pinning centers (Section III), and we compare experimental results with theoretical models in Section IV.

II. THEORETICAL MODELS

A. Primal model (PM)

This model works in the so-called single-vortex approximation; i.e., the vortex is in the anisotropic pinning potential but does not interact with other vortices. It is assumed that the vortex is sufficiently rigid and reacts to external excitation as a whole; therefore, a particle-like equation of motion is used to describe the vortex dynamics. Then the balance of forces of a moving vortex is given as follows:

$$\vec{f_l} + \vec{f_p} + \vec{f_g} = \eta\vec{v} \tag{4}$$

where $\vec{f_l} = [\vec{j} \times \vec{\Phi_0}]$ – force acting on the vortex from the side of the transport current $\vec{j}$; $\vec{\Phi_0}$ - vector along the magnetic field with a value equal to the magnetic flux quantum; η – coefficient of viscous friction due to energy dissipation caused by the generation of an electric field; $\vec{f_p}$ – isotropic component of the pinning force directed opposite to the vortex velocity $\vec{v}$; $\vec{f_g}$ – anisotropic component of the pinning force perpendicular to the easy motion direction.

Let the sample be sliced so that the direction of the transport current makes an angle Ξ with the direction of the vortex easy motion (Fig. 2). For low enough current densities, the driving force $\vec{f_l}$ is small, and the perpendicular to $\vec{f_g}$ component $f_l \sin\Xi$ can be fully balanced by $\vec{f_p}$. In this case, the vortex is being pinned. The start of the vortex motion is possible in one of two scenarios.

1) If the force $\vec{f_g}$ is relatively large, then when $f_l \sin\Xi$ exceeds the maximum value of f_p the vortex begins to move in the direction of easy motion (Fig. 2a). Then, with a further increase of f_l, when the component $f_l \cos\Xi$ exceeds the maximum value of f_g, the vortex acquires a component of velocity perpendicular to the easy motion direction (the slipping effect).
2) If the force $\vec{f_g}$ is relatively weak, then the vortex begins to move in the direction of the sum of forces $\vec{f_l} + \vec{f_g}$ (Fig. 2b). Accordingly, a further increase in the current will lead to a decrease in the guiding effect, since $\vec{f_g}$ is unchanged and $\vec{f_l}$ increases linearly.

The PM model predicts that the choice between the two abovementioned scenarios is determined by the ratio value of the maximum values f_p/f_g compared to $\tan\Xi$. At $f_p/f_g < \tan\Xi$ the first scenario is realized; otherwise the second one. The guiding angle β, at $\Xi \neq 0°, 90°$ is defined as [13]:

$$\begin{cases} \beta = 90° - \Xi, & \text{at complete guiding} \\ \beta = \operatorname{atan}[\dfrac{j}{j_s}\cos\Xi \sin\Xi - \dfrac{1}{\tan\Xi}], & \text{at slipping effect} \end{cases} \tag{5}$$

where j_s – current density at which the slipping effect begins.

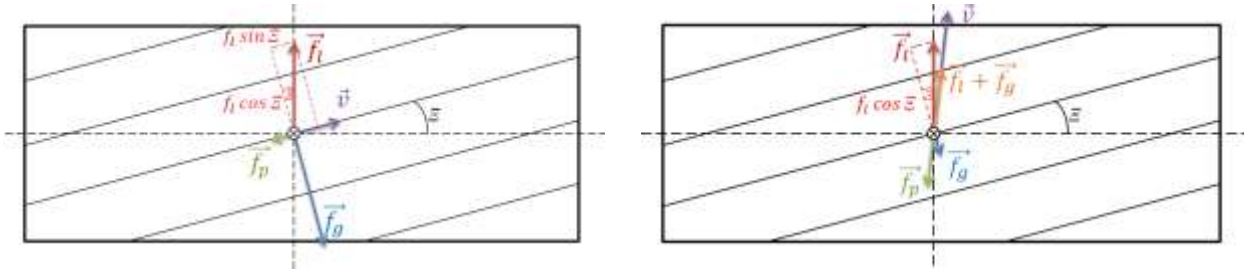

a b

Fig. 2 Force diagrams in the model by Niessen et. al. [13] : a) The case $f_p/f_g < \tan \Xi$. The vortex begins to move along the direction of easy motion, b) The case $f_p/f_g > \tan \Xi$. Immediately at the beginning of movement, the vortex has a velocity component perpendicular to the easy motion direction.

In the experiments of Niessen et al., the components $E_{\parallel}$ and $E_{\perp}$ of the electric field were measured depending on the value of the current, i.e. in the so-called two-dimensional current-voltage characteristics (2D-CVC) regime. One can calculate the angle β according to (3), which is equal to zero in the absence of the guiding effect. In order to be sure that the entire vortex matter was involved in motion, the top parts of the CVCs (with voltage exceeding standard criteria for the critical current ~ 1 μV/cm by 3-4 orders of magnitude) were used. It was experimentally found that angle β changes significantly when the magnetic field H changes. However, this phenomenon was not explained quantitatively within the framework of the primal model. In addition, the experiments have shown that slipping is a much more common phenomenon than the model predicts: complete guiding, i.e., movement only along the easy motion direction is quite rare.

B. Stochastic model (SM)

For a better fit with experimental data, Mawatari proposed to include thermal fluctuations into consideration using the Fokker-Planck mathematical apparatus [20, 21]. This model was later developed in the works of Shklovskij et al. [22, 23, 24, 25, 26] and was called the stochastic model (SM).

This SM model works with similar approximations as the primal model (PM). The balance of forces of a moving vortex is written as:

$$\overrightarrow{f_l} + \overrightarrow{f_p} + \overrightarrow{f_g} + \vec{f}_{th} = \eta \vec{v}. \tag{6}$$

In contrast with the primal model (4) $\vec{f}_{th}$ is added here - the force determined by thermal fluctuations. It assumed that $\vec{f}_{th}$ is a stochastic force, i.e. random with properties defined on average:

$$< f_{th,i} >=0 \tag{7a}$$

$$< f_{th,n}(t) f_{th,m}(t') >= q\delta_{nm}\delta(t-t') \tag{7b}$$

where q – thermal noise magnitude, <…> - statistical averaging, $i,n,m = x,y$ – force components $\vec{f}_{th}$, t – time, $\delta(...)$ – delta function, δ_{nm} - Kronecker symbol (1 if $n = m$, 0 if $n \neq m$).

Equation (7a) means that the force of thermal fluctuations is zero, while condition (7b) means that there are no correlations between different components of the force and the magnitudes of the forces at different moments of time; i.e., fluctuations are white noise. The quantity q is assumed to be defined by temperature T.

Further, taking into account the stochastic nature of the force $\vec{f}_{th}$, one can proceed to a probabilistic description of the vortex dynamics within the framework of the Fokker - Planck equation:

$$\eta \vec{S} = \left(\overrightarrow{f_l} + \overrightarrow{f_p} + \overrightarrow{f_g}\right)P - k_B T \nabla P \tag{8}$$

where k_B – Boltzmann constant. Equation (8) operates with $P(\vec{r},t)$ – the probability density to find the vortex at time t at point $\vec{r} = (x,y)$ and $\vec{S}(\vec{r},t) \equiv P(\vec{r},t)\vec{v}(\vec{r},t)$ is the probability flux density of the vortex. These quantities are related as:

$$\frac{\partial P}{\partial t} = -\nabla \vec{S} \tag{9}$$

The average vortex velocity $< \vec{v} >$, which determines the electric field in accordance with (2), can be found by:

$$< \vec{v} >= \frac{\iint \vec{S} d^2\vec{r}}{\iint P d^2\vec{r}} \tag{10}$$

The last term in Eq. (8) has a clear physical meaning: the temperature equalizes the gradient of vortex concentration the more intense, the higher the temperature. The real influence of this effect can be estimated by comparing the thermal energy $k_B T$ with the energy gain from the vortex pinning effect:

$$u_p \approx r_p f_p \tag{11}$$

where r_p - the typical vortex displacement at which the pinning center ceases to act on the vortex.

In many cases, at sub-LN2 temperatures $\frac{k_B T}{u_p} \sim 10^{-2} \cdots 10^{-6}$. This casts doubt on the adequacy of the explanation of the slipping effect by temperature. In their work [24] Shklovskij et al. noted that, apparently, the stochastic model is not applicable for low-temperature superconductors, leaving a certain narrow region $(T_c - T) \ll T_c$ in which this approach may still be legitimate. However, in this region, the electrodynamics is determined mostly by material inhomogeneity [27, 28, 29, 30], up to the absence of vortices in this temperature region [31, 32, 33]. A detailed review of the objections to the paradigm concerning thermal fluctuations in the electrodynamics of practical superconductors can be found in the work [34].

If one rejects the hypothesis of thermal fluctuations, the question remains: what makes the vortices move perpendicular to easy motion? Both the primal model and the stochastic model use the single-vortex approximation. But strong dependence of the guiding angle on the magnetic field discovered in the first works [13] points to a key role of vortex interaction. Some attempts were made to account for this interaction within the framework of single vortex dynamics by adding the force $\vec{f}_{vv}^{\,i}$ into (4) or (6), acting on the i-th vortex from the rest (see for example [35, 36]). However, due to too many independent fitting parameters, it was not possible to obtain any qualitatively new results in comparison with the already available ones. Even the problem of calculating the bulk pinning force from known pins concentrations and individual pinning forces is difficult, known as the summation problem [37]. The variety of dynamic modes in the presence of correlated pinning centers [38] makes this approach much more laborious.

C. Anisotropic Pinning Model (APM)

At one time with the work of Mawatari [20] an alternative approach to the electrodynamics of superconductors was proposed [10], taking into account the vortex interaction, avoiding the summation problem. Below we describe the general outline of this model. For more details one can refer to the original work [10] or to the review [39] .

The anisotropic pinning model works in the critical state approximation. In this model, an ensemble of a sufficiently large number of vortices is considered as a certain media located in a cooperative energy potential well caused by the entire ensemble of pinning centers at once. In the absence of the transport current, this ensemble of (deformed) vortices occupies the most advantageous place at the well bottom. The minimum of the total specific energy at rest is the result of a balance of energy gain due to pinning of vortices and energy loss due to lattice deformation. Under the influence of a transport current, an ensemble of vortices is jostled along the side of the well. If force (1) exceeds the maximum slope value of the well, the ensemble starts to move. This leads to the generation of the electric field and energy dissipation. Let's define the maximum pinning force of the ensemble of vortices as:

$$\vec{F}_p = -\max\left(\frac{\partial U}{\partial \vec{l}}\right) = -\vec{e}_l \frac{U_0(\vec{B})}{L_0(\vec{j}, B)} \tag{12}$$

where U – the depth of the cooperative potential well, $\vec{e}_l$ – is the unit vector in the direction of the driving force (1), $L_0(\vec{j}, B) = \frac{U_0(\vec{B})}{|\max\left(\frac{\partial U}{\partial l}\right)|}$ is the effective width of the cooperative potential well, $U_0(\vec{B})$ — the effective depth of the cooperative potential well.

An essential assumptions of the model are: 1) that the effective depth of the cooperative potential well $U_0(\vec{B})$ is assumed to depend only on magnetic induction vector $\vec{B}$ (value and direction) and does not depend on the current density $\vec{j}$ and driving force (1); 2) that the effective width of the cooperative potential well $L_0(\vec{j}, B)$ assumed to depend on driving force direction (1) (which always perpendicular to $\vec{B}$) and the absolute value of the magnetic induction $|\vec{B}|$ but does not depend on the direction of magnetic induction.

According to this model, all pinning features (including pinning anisotropy) in a particular material at certain fields are determined by the specific angular dependences of the depth U_0 and the width L_0. In the

case of Nb-Ti cold-rolled tape, the extreme values of U_0 and L_0 are achieved with orientations of magnetic induction and driving force along the main orthogonal directions in the material: normal direction (ND), rolling direction (RD) and direction perpendicular to rolling in the plane of the tape (PD). For other directions, U_0 and L_0 smoothly vary from minimum to maximum. Thus, the depth U_0 and the width L_0 are described by ellipsoids [10]:

$$(\frac{\cos\alpha''}{U^{RD}})^2 + (\frac{\cos\beta''}{U^{PD}})^2 + (\frac{\cos\gamma''}{U^{ND}})^2 = \frac{1}{U_0^2} \tag{13a}$$

$$(\frac{\cos\alpha'}{L^{RD}})^2 + (\frac{\cos\beta'}{L^{PD}})^2 + (\frac{\cos\gamma'}{L^{ND}})^2 = \frac{1}{L_0^2} \tag{13b}$$

where $\cos\alpha''$, $\cos\beta''$, $\cos\gamma''$ – are the direction cosines of induction $\vec{B}$; $\cos\alpha'$, $\cos\beta'$, $\cos\gamma'$ are the direction cosines of the driving force vector; U^{RD}, U^{PD}, U^{ND}, L^{RD}, L^{PD}, L^{ND} depth and width of the cooperative potential well in the main orthogonal directions. In the trivial case of isotropic pinning $U^{RD} \equiv U^{PD} \equiv U^{ND}$ and $L^{RD} \equiv L^{PD} \equiv L^{ND}$.

Let the external magnetic field be normal to the superconductor tape, so $\vec{B} = (0,0,B)$ (Fig. 1). Then, in accordance with (13a) $U_0 = U^{ND}$. This direction of induction corresponds to the two-dimensional cross-section of the ellipsoid L_0, which is determined by all possible directions of the force $\vec{F}$. One can see from (1) for fixed direction of $\vec{B}$ that direction of the force $\vec{F}$ is determined by the current density direction. Thus, we have obtained the conditions for the angles of the direction cosines $\gamma' = 90°$ and $\beta' = 90° - \alpha'$, so from (13b) we get:

$$L_0(\alpha') = \frac{L^{RD}L^{PD}}{\sqrt{(L^{RD}\sin\alpha')^2 + (L^{PD}\cos\alpha')^2}} \tag{14}$$

Then, in accordance with (12):

$$(F_p(\alpha'))^2 = \left(\frac{U^{ND}}{L^{RD}}\right)^2 \cos^2\alpha' + \left(\frac{U^{ND}}{L^{PD}}\right)^2 \sin^2\alpha' \tag{15}$$

Figure 3 presents the angular dependence of the pinning force (15) and gives a simple explanation of the guiding effect. Let the direction of the transport current in the material be such that the driving force (1) is directed along the segment ***ac*** and makes an angle Ξ with the PD-direction. As the values of the pinning force are different for different directions (15) there are directions for which the pinning force magnitude is small enough that the force (1) projection on this direction reaches a critical value earlier (at lower currents) than in the force (1) direction. This corresponds to the achievement of the driving force value ***ab*** in the ***ac*** direction (Fig. 3): the projection ***ad*** reaches the critical pinning value, while the critical value has not yet been reached in the ***ac*** direction (***ab*** < ***ac***). As a result, the vortex matter starts to path not along the action of driving force (1), but along the minimal projection of this force with some angle β to driving force (1). This ultimately leads to the observed deviation of the electric field vector (2) from the current direction by the same angle β. In fig. 3, the dashed line shows the calculated locus of points corresponding to the appearance of such critical projections in the model of a double-ellipsoidal potential well. This curve is an ellipse with principal radii $\frac{U^{ND}}{L^{RD}}$ and $\frac{U^{ND}}{L^{PD}}$ [10].

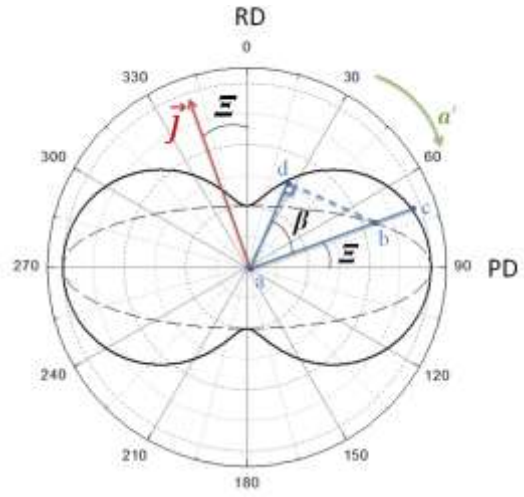

Fig. 3 Diagram of the guiding effect origin in the framework of anisotropic pinning model [10]. The solid line corresponds to anisotropic pinning (15) described by two ellipsoids (13). The dotted ellipse corresponds to the appearance of the first critical projection when the driving force (1) increases.

Taking into account that $\alpha' = 90^0 - \Xi$, we get:

$$F_p(\Xi) = F_p^{PD}\sqrt{\cos^2\Xi + \gamma^2 \sin^2\Xi} \tag{16}$$

where $\gamma = \frac{L^{RD}}{L^{PD}} = \frac{F_p^{PD}}{F_p^{RD}}$ – anisotropy factor determining the guiding angle β:

$$\beta = \operatorname{atan}[\frac{\tan\Xi}{\gamma^2}] - \Xi \tag{17}$$

Thus, in this model, the effect of guided flux flow is the result of the combined action of the anisotropic pinning system and inter-vortex interaction. The latter is taken into account since the factor γ is allowed to vary depending on the magnitude of the magnetic field. Note that the model does not require an assumption about significant influence of thermal fluctuations. The low-field guiding angle predicted by this model was recently confirmed on cold-rolled Nb-Ti tape using magneto-optical studies [40]. This model is also useful for analyzing the critical current angular dependences of superconducting tapes [41].

A similar geometric approach for interpreting the guided flux motion was also proposed in later works by Brandt and Mikitik [42, 43]; however, the first assumption that the pinning force is determined by single ellipsoid did not allow the authors to achieve a plausible guiding angle. For better agreement with the experiment, the authors then modernized the model to describe the angular dependence of the pinning force by a formula similar to (15) [43], however, they did not explain the origin of such a form. In the APM model, the fundamental need for two ellipsoids is due to the fact that pinning force demonstrates bifrontal features of anisotropy: i) with respect to the magnetic field direction at fixed driving force (1) direction, ii) with respect to the driving force (1) direction at a fixed magnetic field direction.

III. EXPERIMENTS

A. Sample and experimental techniques

The samples were fabricated from wide (80 mm) and thin (10 microns) Nb-Ti tape. This object for research was chosen mainly for two reasons. First, Nb-Ti alloy is the most common practical superconducting material with uniform and reproducible properties due to well-developed production. Secondly, in Nb-Ti alloys the upper critical field is about 12 T (at 4.2 K) so the entire field range can be investigated by standard laboratory research equipment.

Compared with previously studied samples [10, 40], here we present the new results for the Nb-Ti tape additionally heat-treated at 385^0C for 25 hours. Previously, we studied in detail the microstructure of the tape, both by electron microscopy and by diffraction methods using X-ray laboratory facilities and synchrotron radiation sources [32, 40]. Relevant microstructure features are presented below in this section.

In cold-rolled tape, the grain boundaries are the main pinning centers. The typical sizes of Nb-Ti grains are ~ 40 nm in the normal direction, ~0.2 μm in the direction perpendicular to rolling, and more than ~1 μm in the rolling direction. As a result of heat treatment, a significant change in grain size was not observed, but ~ 6 vol.% of non-superconducting α-Ti particles, which are effective pinning centers, were precipitated at grain boundaries region. The size distribution of α-Ti particles is well approximated by a lognormal distribution with the most probable sizes of 16 nm in the normal direction (ND), 40 nm in the PD direction and 75 nm in the rolling direction. Such structural changes did not lead to a significant change in the values of the thermodynamic critical parameters (T_c and B_{c2}) and their spread over the tape width (<1%) as compared to cold-rolled tape. However, the width of the critical temperature transition increased by 1.5 times, which indicates an increase in micro inhomogeneity with unchanged macro inhomogeneity.

In addition, the motion of the vortex matter, especially in low fields, is affected by tape thickness variations, which inevitably arise during the rolling process. Surface topography was studied earlier using atomic force microscopy (AFM) [44]. It was found that the tape had micro-scratches along the rolling direction (Fig. 4). The difference in the heights of the tape surface did not exceed 1 μm, with a mean square deviation of 0.24 μm [44].

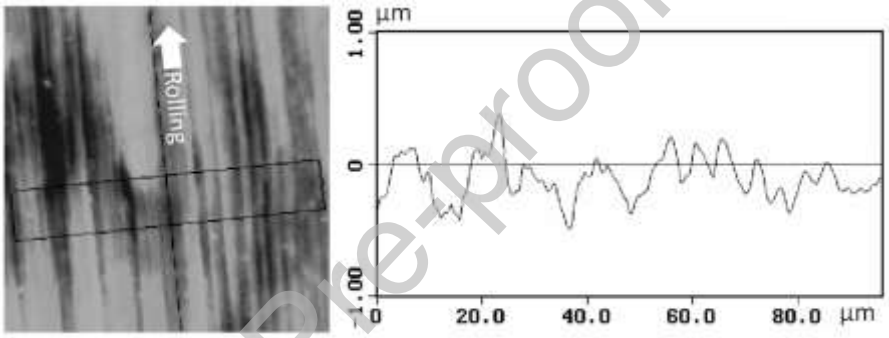

Fig. 4. On the left is the topography of the surface of the Nb-Ti tape, obtained via AFM. The direction of rolling is indicated by an arrow. Changes in the micro relief in the transverse direction are shown in the figure on the right.

For the presented work, samples were sliced at angles Ξ=0^0, 30^0, 60^0, and 90^0 to the rolling direction. To study guided flux motion, a 6-terminals transport method was used: 2 current terminals and 4 voltage terminals soldered in two pairs. The terminals in each pair are located on opposite edges of the sample. This geometry makes it possible to control the lateral Hall-like electric field component at two different locations in the sample. The distance between the terminals in a pair is 3.5 mm; the distance between pairs along the sample is 8 mm. The error in the accuracy of the terminals arrangement in a pair was controlled by voltage measurements in the normal state in the magnetic field higher than H_{c2}. The value of the mismatch of the transverse terminals obtained in this way was taken into account in further measurements. The measurement temperature was 4.2 K. The critical current I_c was determined at 1 μV / cm.

The enhanced current-carrying capacity of the heat-treated samples as compared to the original cold-rolled ones led to thermal instability. For the present study, the samples had a copper shunt layer. This, however, means that when a finite voltage appears across the superconductor, part of the current will be redistributed into the stabilizing layer. To make the effect of current redistribution small, studies were carried out in the range of resistances not exceeding 10% of the resistance in the normal state.

B. Results

Figure 5 shows the field dependences of the volume pinning force defined as $F_p(H) = j_c(H)\mu_0 H$ for heat treated samples sliced at different angles to rolling direction ($\Xi = 0^0, 30^0, 60^0, 90^0$) and for cold

rolled tape in two cases: $\Xi = 0^0$ and 90^0, for comparison. All $F_p(H)$ dependences strongly differ from the typical dome-shaped one, which is usually attributed to strong pinning. In the middle range of fields ($\sim 0.5\,T < \mu_0 H < \sim 8.5\,T$) the pinning force increased for all heat-treated samples compared to cold rolled ones. This behavior is consistent with the known data on the enhancement of pinning during heat treatment [45, 46]. The double-humped shape of the $F_p(H)$ dependence became less pronounced in case of heat treated tape. The appearance of two peaks is often interpreted as a field-induced crossover from the strong to the weak regimes of pinning [47, 48]. It is considered that at low ($\mu_0 H < \sim 1\,T$) and high ($\mu_0 H > \sim 9\,T$) fields the vortex lattice is deformed plastically which leads to the strong pinning regime (can also be called the plastic state of the vortex matter), while in an intermediate field the elasticity of the vortex lattice dominates over the pinning force, resulting in the weak collective pinning (elastic state).

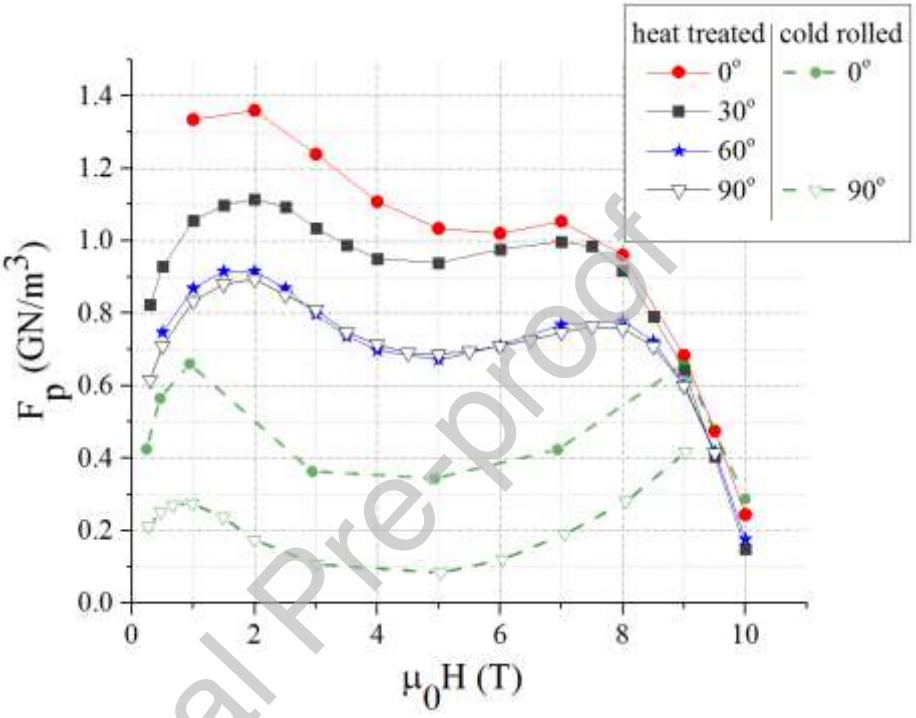

Fig. 5 Field dependence of the pinning force for heat-treated and cold-rolled Nb-Ti tapes for samples sliced at different angles (see legend) to the rolling direction. The magnetic field is normal to the tape.

After heat treatment, not only the increase in the pinning force is observed, but also a significant decrease in the pinning force anisotropy. Figure 6 shows the field dependence of the anisotropy factor, which is defined as a ratio for cases when the sample is sliced across ($\Xi = 90^0$) and along ($\Xi = 0^0$) to the rolling direction $\gamma(H) = \frac{F_p^{\Xi=90}}{F_p^{\Xi=0}}$.

Above the critical current value j_c well detectable electric field appears. From the experimental 2D-CVC it is possible to extract the guiding angle according to (3). Figures 7 and 8 show the guiding angle dependences $\beta(I) = \mathrm{atan}\frac{E_\perp(I)}{E_{||}(I)}$ for samples sliced at angles 30° and 60° respectively. Two solid lines correspond to the two pairs of transverse voltage terminals as described in Section III.A. Registration of the $\beta(I)$ dependence stopped either with a violation of the *I*-V characteristic due to magnetic flux jumps, or reaching 10% of the normal resistance. At low current, the high noise level for $\beta(I)$ observed due to low voltage level.

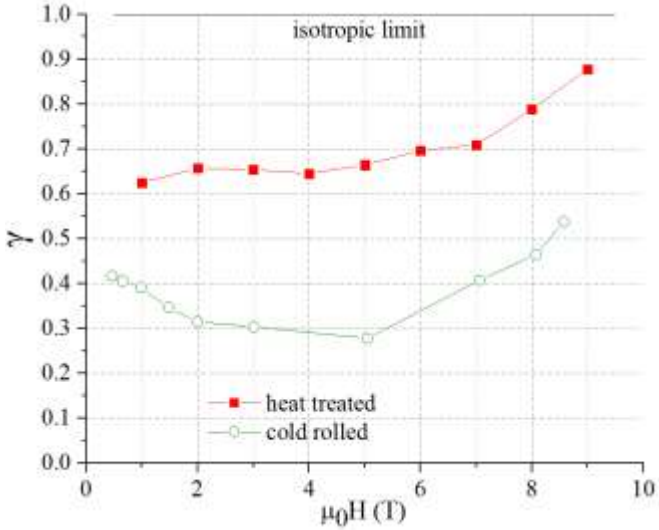

Fig. 6 Field dependence of the pinning force anisotropy factor defined as $\gamma = \frac{F_p^{\Xi=90}}{F_p^{\Xi=0}}$

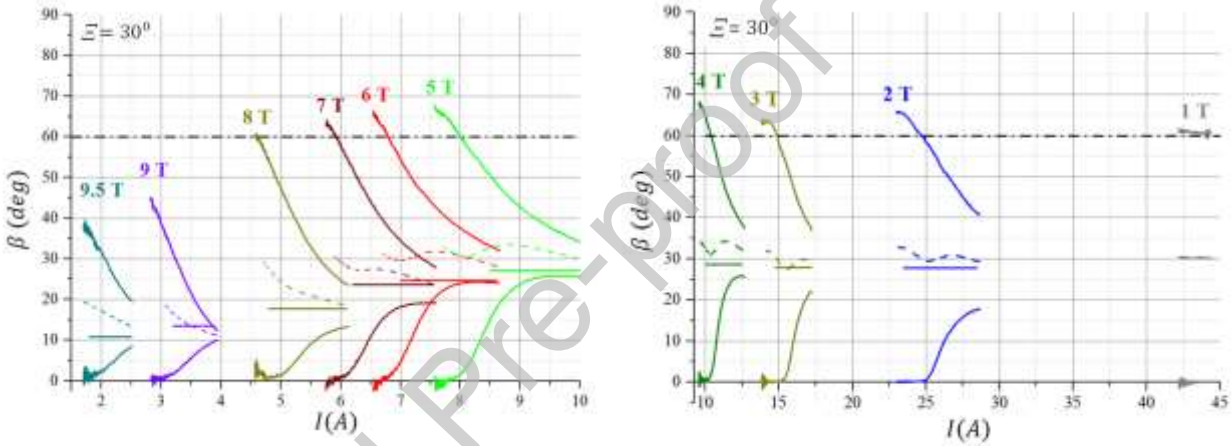

a b

Fig. 7 Guiding angle $\beta(I)$ for the sample cut at an angle $\Xi = 30°$ at different fixed magnetic fields: a) 9.5T – 5T; b) 4T – 1T. The solid lines show the experimental data for two transverse pairs of terminals, the dashed line is the averaging of these two pairs. Horizontal lines are model predictions (17), horizontal black dash-and-dot lines correspond to full guiding.

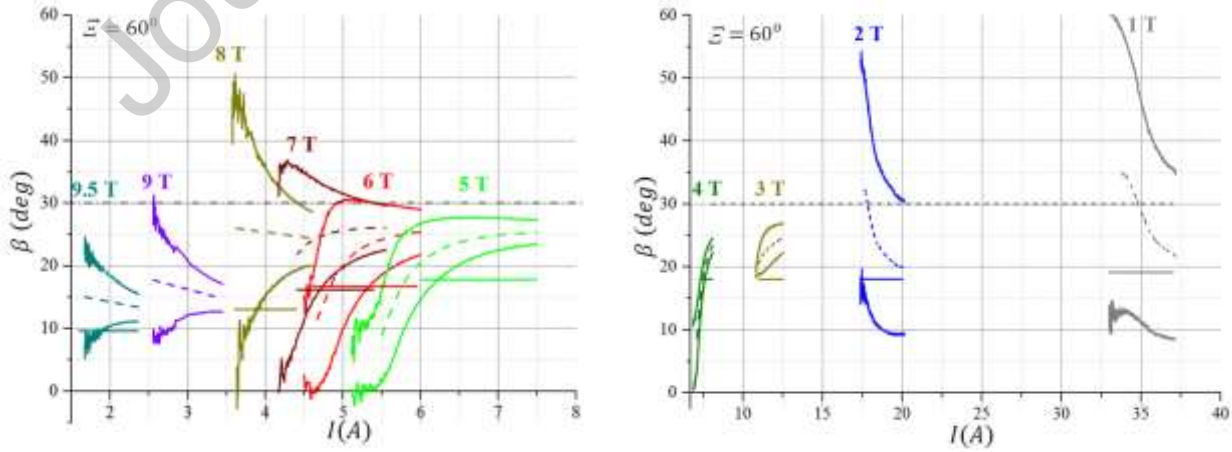

a b

Fig. 8 Guiding angle $\beta(I)$ for the sample cut at an angle $\Xi = 60°$ at different fixed magnetic fields: a) 9.5T – 5T; b) 4T – 1T. The solid lines show the experimental data for two transverse pairs of terminals, the dashed line is the averaging of these two pairs. Horizontal lines are model predictions (17), horizontal black dash-and-dot lines correspond to full guiding.

For convenience Figures 7 and 8 also show the angels corresponding to the full guiding, i.e. no slipping effect (black dash-and-dot line), and guiding angles expected in the AMP model (solid horizontal lines).

Note that in all experiments the curves in Figures 7 and 8 are fully reproduced with an increase and decrease of the transport current, which indicates that the magnetic flux in both cases moves along the same trajectories.

IV. DISCUSSIONS

At low magnetic field, the vortex interaction is relatively small. The anisotropy factor defined in terms of the volume pinning force F_p can be approximately expressed as $\gamma|_{H\to 0} \approx \frac{f_p}{f_p+f_g}$, where f_p and f_g – isotropic and anisotropic components of the elemental pinning force in equation (4). Thus, from the data in Figure 6, one can estimate the ratio included in the Primal model (PM) as $f_p/f_g \approx 1.5$. This ratio is greater than $\tan(30°) = 0.577$, but less than $\tan(60°) = 1.732$, and therefore in accordance with the PM predictions for the angle Ξ = 30° the slipping effect is realized, while at the angle Ξ = 60° the compete guiding should be observed. However, it is clearly seen from Figures 7 and 8 that complete guiding is not realized for Ξ = 30° nor for Ξ = 60°.

The value of the elemental pinning force was estimated earlier for cold-rolled tape [48]. Estimates made within the framework of various models were in good agreement and for the elemental energy of pinning gave the value $u_p \approx 150\ K$ [48]. Since the grain sizes did not change after heat treatment, there was no increase in the concentration of pinning centers. On the other hand, as can be seen from Figure 5, the volume pinning force has increased after heat-treatment, which indicates an increase in the energy of vortex capture u_p. Hence, the value $u_p \approx 150\ K$ can be used as a lower estimate for elemental pinning in the heat-treated tape. Thus, the ratio $\frac{k_B T}{u_p}$ is not more than 3% and it is hard to believe that the pronounced slipping effect can be explained by thermal fluctuations in this case.

The Anisotropic Pinning Model (APM) gives the most accurate predictions for the guiding angle values and its dependence on the magnetic field, which can be considered semi-quantitative (Fig. 7 and Fig. 8). The critical state approximation was justified for cold-rolled tape with weak pinning, since it did not show a significant dependence of the guiding angle on the current value [10]. On the contrary, for the heat treated tape at low electric field values (near the criterion $E_c = 10^{-4}\ V/m$), the guiding angle is not the same in different locations of the tape. This can be interpreted as the plastic nature of the vortex matter motion, i.e. vortices can exchange neighbors while moving. In other words, due to the inhomogeneity of the pinning landscape, percolation paths appear in the vortex matter, so some chains of vortices are moving while the rest of the vortex matter is motionless [49, 50]. Thus, the heat treatment leads to an increase in pinning strength and to crossover from elastic to plastic flow modes, which is also consistent with well-known trends [51]. At higher voltages, the effective pinning forces experienced by the moving vortex matter become weak enough that the vortex matter can dynamically form a moving, elastically deformed solid [52]. This corresponds to the meeting tendency for each two branches in Figures 7 and 8 at high currents.

The above reasoning explains why, in the plastic flow mode, the prediction of the guiding angel in the APM model can be correct only on average while the elastic flow regime is much better in agreement with the model.

To conclude this section, we would like to note that several simulations have been performed to investigate the influence of the plastic-elastic flow crossover on the guiding effect [52, 53]. The presented experimental data can serve as a guideline for further work on this kind.

V. CONCLUSION

This article presents the experimental results of the guiding angel in the case of the Nb-Ti tape with strong pinning centers of low concentration. When the generated electric field is small enough, the

guiding angle varies significantly at different locations along the sample, which corresponds to the plastic mode of the vortex matter motion. With an increase in the transport current, the guiding angle becomes more uniform, which indicates the coherent motion of the vortex matter.

The article reviews models capable of predicting the guided motion angle and discusses the limitations of the models. It is shown that in the case of superconductors with strong dilute pinning centers, the anisotropic pinning model is closest to experimental observations. In this framework, the slipping effect is the result of the combined action of the vortex interaction and the anisotropy of the pinning centers. This model describes semi-quantitatively the field dependence of the guiding angle for Nb-Ti tape in case of weak collective pinning, as well as in the case of strong pinning and the elastic mode of the vortex matter motion, which is realized at high enough driving force. In the case of plastic flux flow mode, this model predicts the guiding angle as averaged over the sample length.

The work was supported by NRC "Kurchatov Institute".

Valentin Guryev: Conceptualization, Formal analysis, Investigation, Resources, Writing - Original Draft, Visualization.

Sergey Shavkin: Methodology, Software, Investigation, Writing- Reviewing and Editing

Vitaliy Kruglov: Supervision, Writing- Reviewing and Editing

The authors do not have any conflict of interest to declare.

The authors have no affiliation with any organization with a direct or indirect financial interest in the subject matter discussed in the manuscript.

This manuscript is not under review at any other journal.

References

[1] Wendin G. Quantum information processing with superconducting circuits: a review. *Rep. Prog. Phys.* 80 (2017) 106001. https://doi.org/10.1088/1361-6633/aa7e1a

[2] Arute F., Arya K., Babbush R. et al. Quantum supremacy using a programmable superconducting processor. *Nature* 574 (2019) https://doi.org/10.1038/s41586-019-1666-5

[3] Silhanek A.V., Van de Vondel J., Moshchalkov V.V. Guided Vortex Motion and Vortex Ratchets in Nanostructured Superconductors. [book auth.] Wordenweber R., Lang W. Moshchalkov V. *Nanoscience and Engineering in Superconductivity.* Heidelberg Dordrecht London New York : Springer, 2010 https://doi.org/10.1007/978-3-642-15137-8_1

[4] Dobrovolsky O.V. Abrikosov fluxonics in washbroad nanolandscapes. *Physica C.* 533 (2017) 80-90. https://doi.org/10.1016/j.physc.2016.07.008

[5] Dobrovolskiy O.V., Begun E., Bevz V.M., Sachser R., Huth M. Upper Frequency Limits for Vortex Guiding and Ratchet Effects. *Physical review applied.* 13 (2020) p. 024012 https://doi.org/10.1103/PhysRevApplied.13.024012

[6] Vlasko-Vlasov V.K., Colauto F., Buzdin A.I., Rosenmann D., Benseman T., Kwok W.-K. Manipulating Abrikosov vortices with soft magnetic stripes. *Phys. rev. B.* 95 (2017) 174514 https://doi.org/10.1103/PhysRevB.95.174514

[7] Vlasko-Vlasov V.k., Colauto F., Buzdin A.I., Rosenmann D., Benseman T., Kwok W.-K. Magnetic gates and guides for superconducting vortices. *Phys. rev. B.* 95 (2017) 144504. https://doi.org/10.1103/PhysRevB.95.144504

[8] Wordenweber R. Engineering of superconductors and superconducting devices using artificial pinning sites. *Physical Sciences Reviews.* 2 (2017) 20178000. https://doi.org/10.1515/psr-2017-8000

[9] Wördenweber R. Artificial pinning sites and their applications. [book auth.] Moshchalkov V., Bending S., Tafuri F. Wördenweber R. *Superconductors at the Nanoscale.* Berlin/Boston : Walter de Gruyter GmbH, 2017 https://doi.org/10.1515/psr-2017-8000

[10] Klimenko E.Yu., Shavkin S.V., Volkov P.V. Anisotropic pinning in macroscopic electrodynamics of superconductors. *Zh. Eksp. Teor. Fiz.* 1997, Vol. 112, pp. 1055-1081. https://doi.org/10.1134/1.558341.

[11] Yu Liu, Xiao-Fan Gou, Feng Xue. Barrier or easy-flow channel: The role of grain boundary acting on vortex motion in type-II superconductors. *Chin. Phys. B.* 30 (2021) 9. https://doi.org/10.1088/1674-1056/ac11ea

[12] Staas F.A., Niessen A.K., Druyvesteyn W.F., Suchtelen J.V. Guided motion of vortices in type II superconductors. *Physical letters.* 13 (1964) 4. https://doi.org/10.1016/0031-9163(64)90014-9

[13] Neessen A.K., Weijsenfeld C.H. Anisotropic Pinning and Guided Motion of Vortices in Type-II Superconductors. *Journal of applied physics.* 40 (1969) 1. https://doi.org/10.1063/1.1657066

[14] Villegas J.E., Gonzalez E.M., Montero M.I., Schuller I.K, Vicent J.L. Vortex-lattice dynamics with channeled pinning potential landscapes. *Physical review B.* 72 (2005) 064507. https://doi.org/10.1103/PhysRevB.72.064507

[15] Kokubo N., Besseling R., Vinokur V.M., Kes P.H. Mode Locking of Vortex Matter Driven through Mesoscopic Channels. *Physical review letters* 88 (2002) 24 https://doi.org/10.1103/PhysRevLett.88.247004

[16] Wordenweber R., Dymashevski P. Guidance of vortices and the vortex ratchet effect in high-Tc superconducting thin films obtained by arrangement of antidots. *Physical review B.* 69 (2004) 184504. https://doi.org/10.1103/PhysRevB.69.184504

[17] Kopelevich Ya.V., Lemanov V.V., Sonin E.B., Kholkin A.L. Even Hall effect in superconducting phase of YBa2Cu3O7-x. *Pis'ma Zh. Eksp. Teor. Fiz.* 50 (1989) 188-191. http://jetpletters.ru/ps/1127/article_17082.pdf.

[18] Pastoriza H., Candia S., Nieva G. Role of Twin Boundaries on the Vortex Dynamics in YBa2Cu3O7. *Physical review lettres.* 83 (1999) 5. https://doi.org/10.1103/PhysRevLett.83.1026

[19] Vasek P., Janecek I., V. Plechacek V. Intrinsic pinning and guided motion of vortices in high-Tc superconductors. *Physica C* 247 (19995) 381-384. https://doi.org/10.1016/0921-4534(95)00212-X

[20] Mawatari Y. Dynamics of vortices in planar pinning centers and anisotropic conductivity in type-II superconductors. *Phys. rev. B.* 56 (1997) https://doi.org/10.1103/PhysRevB.56.3433

[21] Mawatari Y Anisotropic current-voltage characteristics in type-II superconductors with planar pinning centers. *Phys. rev. B.* 9 (1999) 18 https://doi.org/10.1103/PhysRevB.59.12033

[22] Shklovski V.A., Soroka A.K., Soroka A.A. Nonlinear dynamics of vortices pinned to unidirectional twins. *Journal of experimental and theoretical physics* 89 (1999) 6. https://doi.org/10.1134/1.559064

[23] Shklovskij V.A., Soroka A.A. Anisotropy of the critical current and the guided motion of vortices in a stochastic model of bianisotropic pinning. *Low temperature physics* 28 (2002) 4 https://doi.org/10.1063/1.1477358

[24] Soroka O.K., Shklovskij V.A., Huth M. Guiding of vortices under competing isotropic and anisotropic pinning conditions: Theory and experiment. *Physical review B* 76 (2007) 014504. https://doi.org/10.1103/PhysRevB.76.014504

[25] Shklovskij V.A., Sosedkin V.V. Guiding of vortices and ratchet effect in superconducting films with asymmetric pinning potential. *Physical review B* 80 (2009) 214526 https://doi.org/10.1103/PhysRevB.80.214526

[26] Dobrovolskiy O.V., Hanefeld M., Zorb M., Huth M., Shklovskij V.A. Interplay of flux guiding and Hall effect in Nb films with nanogrooves. *Supercond. Sci. Technol.* 29 (2016) 065009 https://doi.org/10.1088/0953-2048/29/6/065009

[27] Segal A., Karpovski M., Gerber A. Inhomogeneity and transverse voltage in superconductors. *Phys Rev. B.* 83 (2011) 094531 https://doi.org/10.1103/PhysRevB.83.094531

[28] Guryev V., Shavkin S., Kruglov V. Inhomogeneity and irreversibility field of superconducting Nb-Ti tapes. *EPJ Web of Conferences* 185 (2018) 08004. https://doi.org/10.1051/epjconf/201818508004

[29] Guryev V.V., Shavkin S.V., Kruglov V.S., Volkov P.V. Superconducting transition of Nb-Ti tape studied by transverse voltage method. *Physica C* 567 (2019) https://doi.org/10.1016/j.physc.2019.1353546

[30] Zhao D., Zhao Zh., Xu Ya, Tong Sh., Lu J., Wei D. Transverse Magnetoresistance Induced by the Nonuniformity of Superconductor . *Nanomaterials* 1313 (2022) https://doi.org/10.3390/nano12081313

[31] Klimenko E.Yu., Shavkin S.V., Volkov P.V. Manifestations of Macroscopic Nonuniformities in Superconductors with Strong Pinning in the Dependences of the Transverse Current-Voltage Curves on the Magnetic Field near Hc2. *Physics of Metals and Metallography* 92 (2001) 6

[32] Guryev V.V., Shavkin S.V., Kruglov V.S., Volkov P.V., Vasiliev A.L., Ovcharov A.V., Likhachev I.A., Pashaev E.M., Svetogorov R.D., Zubavichus Y.V. Apparent anisotropy effects of upper critical field in high-textured superconducting Nb-Ti tapes. *Journal of Physics: Conference Series* 747 (2016) 012034 https://doi.org/10.1088/1742-6596/747/1/012034

[33] Guryev V., Shavkin S., Irodova A., Kruglov V. Abnormal behaviour of the resistive transition to the normal state in superconducting Nb-Ti tapes just below Hc2. *EPJ Web of Conferences* 201 (2019) 02001 https://doi.org/10.1051/epjconf/201920102001

[34] Klimenko E.Yu., Imenitov A.B., Shavkin S.V., Volkov P.V. Resistance–Current Curves of High Pinning Superconductors. *J. Exp. and Theor. Phys.* 100 (2005) 50-65 https://doi.org/10.1134/1.1866198

[35] Zhu B.Y., Dong J., Xing D.Y. Vortex dynamics in twinned superconductors. *Phys. rev. B.* 57 (1998) 9 https://doi.org/10.1103/PhysRevB.57.5075

[36] Lai Jiang, WeiWei Xu, Tao Hua, Mei Yu, DeYue An, Jian Chen, BiaoBing Jin, Lin Kang, PeiHeng Wu . Simulation and experiment of vortex transport properties in a Type II superconductor with grain boundary. *Science China. Technological Science* 58 (2015) 493-498 https://doi.org/10.1007/s11431-014-5731-x

[37] Matsushita T. Flux Pinning Characteristics [book auth.] Matsushita T. *Flux Pinning in Superconductors.* Verlag Berlin Heidelberg : Springer, 2014 https://doi.org/10.1007/978-3-642-45312-0_7

[38] Chaturvedi H., Galliher N., Dobramysl U., Pleimling M., Tauber U.C. Dynamical regimes of vortex flow in type-II superconductors with parallel twin boundaries. *The Eur. Phys. J. B.* 91 (2018) 294 https://doi.org/10.1140/epjb/e2018-90447-3

[39] Klimenko, E.Yu. Electrodynamics of High Pinning Superconductors. [book auth.] A.M. Luiz. *Superconductivity Theory and Applications.* Rijeka : InTech, 2011 https://doi.org/10.5772/21269

[40] Shavkin S., Guryev V., Kruglov V., Ovcharov A., Likhachev I., Vasiliev A., Veligzhanin A., Zubavichus Y. Features of microstructure and magnetic flux dynamics in superconducting Nb-Ti tapes with strong anisotropic pinning. *EPJ Web of Conferences* 185 (2018) 08007 https://doi.org/10.1051/epjconf/201818508007

[41] Guryev V.V., Shavkin S.V., Kruglov V.S. Method for critical current angular dependencies analysis of superconducting tapes. *Journal of Physics: Conference Series* 2103 (2021) 012096. https://doi.org/10.1088/1742-6596/2103/1/012096

[42] Mikitik G.P., Brandt E.H. Flux-line pinning by point defects in anisotropic biaxial type-II superconductors. *Phys. rev. B.* 79 (2009) https://doi.org/10.1103/PhysRevB.79.020506

[43] Mikitik G.P., Brandt E.H. Determination of anisotropic pinning force by measuring critical current density in an inclined magnetic field. *Phys. rev. B.* 83 (2011) 104514. https://doi.org/10.1103/PhysRevB.83.104514

[44] Shavkin S.V., Guryev V.V., Chumakov N.K., Irodova A.V., Kruglov V.S. Anomalous Magnetization Central Peak Shift of Nb-Ti Tapes with High In-Plane Critical Current Anisotropy Journal of Superconductivity and Novel Magnetism (2022) https://doi.org/10.1007/s10948-022-06248-y

[45] Matsushita T., Küpfer H. Enhancement of the superconducting critical current from saturation in NbTi wire. *Journal of Applied Physics* 63 (1988) http://dx.doi.org/10.1063/1.340402

[46] Ionescu A.M., Ivan I., Enculescu M., Grigoroscuta M., Miu D., Valeanu M., Badica P., Miu L. From an Anomalous Peak Effect to a Second Magnetization Peak in Nb-rich Nb-Ti Alloys. *J Supercond Nov Magn.* 2017 30 (2017) 1103-1108. https://doi.org/10.1007/s10948-016-3670-4

[47] Larkin A.I., Ovchinnilov Yu.N. Pinning in type II superconductors. *Journal of Low Temperature Physic* 34 (1979) 3/4 https://doi.org/10.1007/BF00117160

[48] Guryev V.V., Shavkin S.V., Kruglov V.S. Irreversibility field and anisotropic δl-pinning in type II superconductors. *Journal of physics: conference series* 1697 (2020) 012202 https://doi.org/10.1088/1742-6596/1697/1/012202

[49] Gurevich A., Vinokur V.M. Nonlinear Electrodynamics of Randomly Inhomogeneous Superconductors. *Phys. Rev. Lett.* 83 (1999) 15. https://doi.org/10.1103/PhysRevLett.83.3037

[50] Meilikhov E.Z. An even Hall effect in superconductors. *Physica C* 209 (1993) 566-572. https://doi.org/10.1016/0921-4534(93)90576-C

[51] Le Doussal P., Giamarchi T. Moving glass theory of driven lattices with disorder. *Phys. rev. B.* 57 (1998) 18. https://doi.org/10.1103/PhysRevB.57.11356

[52] Reichhardt C., Reichhardt C.J.O. Depinning and nonequilibrium dynamic phases of particle assemblies driven over random and ordered substrates: a review. *Rep. Prog. Phys.* 80 (2017) 026501. https://doi.org/10.1088/1361-6633/80/2/026501

[53] Reichhardt C., Reichhardt C.J.O. Vortex guidance and transport in channeled pinning arrays. *Fiz. Nizk. Temp.* 46 (2020) 377-385 https://doi.org/10.1063/10.0000860.